CHEMISTRY OF MATERIALS
Article

Chem. Mater. **2009,** *21,* 5681–5690 5681
DOI:10.1021/cm9023887

Novel Metastable Hexagonal MoO_3 Nanobelts: Synthesis, Photochromic, and Electrochromic Properties

Lei Zheng, Yang Xu, Dong Jin, and Yi Xie*

Department of Nanomaterials and Nanochemistry, Hefei National Laboratory for Physical Sciences at Microscale, University of Science and Technology of China, Hefei, Anhui 230026, P.R. China

Received August 3, 2009. Revised Manuscript Received October 15, 2009

In this work, we report the crystalline structure, morphology, and optical properties of novel metastable hexagonal phase MoO_3 (*h*-MoO_3) nanobelts prepared by a simple hydrothermal route from peroxomolybdate solution with the presence of sodium nitrate as a mineralizer. During the reaction process, $NaNO_3$ has been proposed to influence the deoxidation, condensation, and further dehydration of the water-soluble peroxomolybdate precursor for connecting the [MoO_6] octahedra with vertex sharing and edge sharing arrangements on determining the generation of metastable phase. The present work comparatively investigates the photochromic and electrochromic behaviors of the resultant hexagonal *h*-MoO_3 nanobelts and the common thermodynamically stable orthorhombic α-MoO_3 nanobelts. The performances concerning photochromism on two types of MoO_3 nanobelt suspensions show that the photochemical efficiency of *h*-MoO_3 is more excellent than that of α-MoO_3 under UV light irradiation based on a remarkable coloration phenomenon. And the as-obtained *h*-MoO_3 nanobelt coated film exhibits a steady electrochromic property in quick response to electrical impulse. Higher structure openness degree in the tunnel structure of *h*-MoO_3, which could lead to an efficient electron−hole separation and provid larger spatial locations for cation insertion/extraction and diffusion, is suggested to be responsible for its enhanced coloration properties.

1. Introduction

A chromogenic material is able to change its optical properties in response to an external stimulus. Well known examples are photochromic, thermochromic, and electrochromic materials, which can be changed in a controlled and reversible manner when there are light, heat, or electrical impulsing, respectively. Thus, the chromogenic materials provide suitable applications in a concept of "smart window", which enables energy exchange through a window in a controllable way and to maximize the energy savings. A smart window glass with utilization of chromogenic materials, by its very definition, implies that it has the unique ability to sense or respond to an external stimulus in a predetermined and adjustable manner. To meet the potential energy saving application, considerable research interests have been focused on developing various organic or inorganic materials possessing the chromogenic properties. Thereinto, transition metal oxides[1−5] have been studied as attractive candidates of chromogenic materials thanks to their fast response, high coloration efficiency and long-term stability, and so forth.

Among the various kinds of chromogenic materials of transition-metal oxides, molybdenum oxide is an ideal research object in the respect that its multiresponse in photochromism,[6] electrochromism,[7,8] and thermochromism[9] is distinctive and intriguing. The chromogenic response of MoO_3 shows a stronger and more uniform absorption of light in its colored state (molybdenum bronze) and also shows a better open-circuit memory than a majority of transition-metal oxides. Moreover, MoO_3 shows great apparent coloration efficiency since molybdenum bronze is more akin to the sensitivity in human visual perception.

Up to the present, all the studies have been carried out on the photochromic and electrochromic applications of the conventional thermodynamically stable phase of MoO_3—orthorhombic α-MoO_3, of which the structure is shown in Scheme 1A,B. It is constituted by [MoO_6] octahedra, with sharing edges and corners, resulting in zigzag chains and unique layers parallel to the (010) plane structure, presenting open channels for H^+ or Li^+ ion intercalation. Molybdenum trioxide has other two meta-

*To whom correspondence should be addressed. Fax: 86-551-3606266. E-mail: yxie@ustc.edu.cn.

(1) Catherine, S.; Richard, J. *J. Mater. Chem.* **2001**, *11*, 815.
(2) Masahiro, M.; Akira, N.; Toshiya, W.; Kazuhito, H. *Chem. Mater.* **2002**, *14*, 2812.
(3) Georg, A.; Georg, A.; Krasovec, U. *Thin Solid Films* **2006**, *502*, 246.
(4) He, T.; Ma, Y.; Cao, Y.; Yang, W.; Yao, J. N. *Phys. Chem. Chem. Phys.* **2002**, *4*, 1637.
(5) Ghicov, A.; Yamamoto, M.; Schmuki, P. *Angew. Chem., Int. Ed.* **2008**, *47*, 7934.
(6) Yang, Y.; Cao, Y.; Loo, B.; Yao, J. N. *J. Phys. Chem. B* **1998**, *102*, 9392.
(7) He, T.; Yao, J. N. J. *Photochem. Photobiol., C: Photochem. Rev.* **2003**, *4*, 125.
(8) Yahaya, M.; Salleh, M.; Talib, A. *Solid State Ionics* **1998**, *113*, 421.
(9) Chudnovskii, F. A.; Schaefer, D. M.; Gavrilyuk, A. I.; Reifenberger, R. *Appl. Surf. Sci.* **1992**, *62*, 145.

Published on Web 11/11/2009

Scheme 1. Schematic Representation of (A, B) Orthorhombic α-MoO_3 and (C, D) Hexagonal *h*-MoO_3 Crystalline Structure

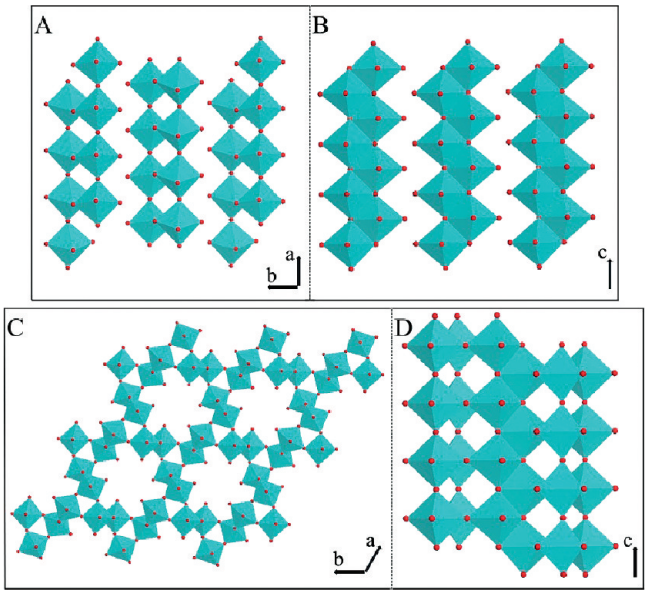

stable phases: monoclinic β-MoO_3 and hexagonal *h*-MoO_3 polymorphs. Monoclinic β-MoO_3 possesses a ReO_3-related structure, where the [MoO_6] octahedra share corners to form a distorted cube. The type of molybdenum oxide interested in this work is hexagonal *h*-MoO_3, which is constructed of the zigzag chains of [MoO_6] octahedra as the building blocks but interlinked through the *cis*-position, giving a hexagonal crystalline structure with large one-dimensional tunnels, as shown in Scheme 1C,D. Its structural characteristics should be taken into account that in between these octahedra, the extended tunnels can serve as conduits and intercalation sites for mobile ions. Though the tunnel structure and the layered structure are spatially open constructions, the materials with tunnel structure generally possess more capaciousness in crystal local structure. And according to the photocatalytic results reported elsewhere,[10] the compounds presenting tunnel structure could contribute to an accelerated electron−hole separation under irradiation, which is regarded as an improved catalytic activity. In this sense, the tunnel structure in *h*-MoO_3 compound here is surmised to facilitate the electron−hole separation and then enhance the photochromic performance compared with the orthorhombic α-MoO_3. Moreover, the research on electrochromism[11] or Li^+ ion batteries[12] demonstrates that the tunnel structure compounds could allow more ions to intercalate and reduce the diffusion/migration barrier for small ions into the host structure, which give us inspiration that the hexagonal *h*-MoO_3 with tunnel structure also facilitates ion insertion/extraction and exhibits a new or excellent electrochromism. Significantly, to obtain the chromogenic materials with tailored coloration properties, the detailed structural dependence between hexagonal and orthorhombic MoO_3 polymorphs must be revealed as a reasonable example. However, the application of *h*-MoO_3 as a chromogenic material as well as the detailed coloration characterization compared to the normal α-MoO_3 has not been studied.

As far as the chemical ways are concerned, α-MoO_3 nanobelts could be readily prepared via several methods,[13−18] while only hexagonal rod/prism-shaped microstructures *h*-MoO_3 have been synthesized[19,20] as a result of its characteristic symmetry. It is known that due to the rectangular cross section and uniform width or thickness, nanobelts could be an ideal system for fully understanding the structure−property relationship in functional oxides. For example, WO_3 nanobelts[21] showed more excellent photocatalytic ability and photoelectrochemical properties than tungsten oxide film. V_2O_5 nanobelts[22] fabricated by our group also indicated that the surface area of the beltlike structures dramatically affect the intercalation rate and capacitance while applied in lithium ion battery. Thus, it is much expected and intriguing to realize that the *h*-MoO_3 sample in beltlike nanostructures exhibits distinct properties in photochromism and electrochromism.

Here, we demonstrate a simple hydrothermal decomposition reaction from prefabricated peroxomolybdate precursor solution to produce high-quality *h*-MoO_3 nanobelts. In the present reaction system, the existence of $NaNO_3$ is proved to influence the deoxidation, condensation, and further dehydration process of the peroxomolybdate precursor for connecting [MoO_6] octahedra with vertex sharing and edge sharing arrangements, so regarded as a crucial mineralizer for the formation of metastable phase *h*-MoO_3. More importantly, our approach offers the first opportunity to investigate the application of metastable phase *h*-MoO_3 nanobelts in photochromism and electrochromism. As expected, the obtained *h*-MoO_3 nanobelts work as a chromogenic material and exhibit considerably higher sensitivity, coloration efficiency, and faster response in compared with the conventional α-MoO_3 nanobelts, which is mainly attributed to the *h*-MoO_3 of tunnel structure with a higher structure openness degree making for an accelerated

(10) Lin, X.; Huang, F. Q.; Wang, W.; Wang, Y.; Xia, Y. J.; Shi, J. *Appl. Catal. A: Gen.* **2006**, *313*, 218.
(11) Balaji, S.; Djaoued, Y.; Albert, A.; Ferguson, R. Z.; Bruning, R. *Chem. Mater.* **2009**, *21*, 1381.
(12) Colin, J. F.; Prolong, V.; Hervieu, M.; Caignaert, V.; Raveau, B. *Chem. Mater.* **2008**, *20*, 1534.
(13) Hu, X. K.; Ma, D. K.; Xu, L. Q.; Qian, Y. T. *Chem. Lett.* **2006**, *35*, 962.
(14) Li, X. L.; Liu, J. F.; Li, Y. D. *Appl. Phys. Lett.* **2002**, *81*, 4832.
(15) Xia, T.; Li, Q.; Liu, X.; Meng, J.; Cao, X. *J. Phys. Chem. B* **2006**, *110*, 2006.
(16) Song, R. Q.; Xu, A.; Deng, B.; Fang, Y. *J. Phys. Chem. B* **2005**, *109*, 22758.
(17) Hu, X. K.; Qian, Y. T.; Song, Z. T.; Huang, J. R.; Cao, R.; Xiao, J. Q. *Chem. Mater.* **2008**, *20*, 1527.
(18) Li, G.; Jiang, L.; Pang, S. P.; Peng, H. R.; Zhang, Z. K. *J. Phys. Chem. B* **2006**, *110*, 24472.
(19) Song, J.; Ni, X.; Gao, L.; Zheng, H. G. *Mater. Chem. Phys.* **2007**, *102*, 245.
(20) Ramana, C. V.; Atuchin, V. V.; Troitskaia, I. B.; Gromilov, S.; Kostrovsky, V.; Saupe, G. *Solid State Commun.* **2009**, *149*, 6.
(21) Wang, H.; Quan, X.; Zhang, Y.; Chen, S. *Nanotechnology* **2008**, *19*, 065704.
(22) Li, B. X.; Xu, Y.; Rong, G.; Jing, M.; Xie, Y. *Nanotechnology* **2006**, *17*, 2560.

electron−hole separation in photochromism and a facile intercalation and diffusion of Li^+ ions in electrochromism. This research on coloration properties between different polymorphs of MoO_3 would present a method to effectively find more alternative chromogenic materials, thereby extending the application to the smart window field.

2. Experimental Section

All chemical reagents in this work were purchased from the Shanghai Chemical Company. They were of analytical grade and used without further purification.

Synthesis of Hexagonal MoO_3 Nanobelts. In a typical procedure, 1.0 g pure Mo powder (10.4 mmol) was slowly added into a beaker containing 10 mL of H_2O_2 aqueous solution (30% w/w) with strong stirring in an ice−water bath. A transparent, yellow solution containing the water-soluble precursor compound $MoO_2(OH)(OOH)$[23] would form. Then 0.5 g of sodium nitrate was dissolved in the peroxomolybdate solution under magnetic stirring to form a homogeneous aqueous solution. Subsequently, the solution was transferred into a Teflon-lined stainless steel autoclave (15 mL) and hydrothermally treated at 150 °C for 12 h. After cooling to room temperature naturally, a yellowish white product of *h*-MoO_3 nanobelts was collected by centrifuging the mixture, washed with distilled water several times, and then dried under a vacuum at 60 °C overnight for further characterization.

Sample Characterization. The samples were characterized by X-ray powder diffraction (XRD) with a Japan Rigaku Dmax X-ray diffractometer equipped with graphite monochromatized high-intensity Cu Kα radiation (λ = 1.54178 Å). The transmission electron microscopy (TEM) images were obtained by a Hitachi Model H-800 instrument with a tungsten filament, using an accelerating voltage of 200 kV. High-resolution transmission electron microscopy (HRTEM) images and electron diffraction (ED) patterns were carried out on a JEOL-2010 transmission electron microscope at an acceleration voltage of 200 kV. The field emission scanning electron microscopy (FESEM) images were taken on a FEI Sirion-200 scanning electron microscope. Thermogravimetric analysis (TGA) and differential scanning calorimetry (DSC) were performed on DTG-60H and DSC-60, respectively. UV−vis spectra were recorded on a Solid Spec-3700 spectrophotometer at room temperature. The periodic first-principles calculations presented here implement in the CASTEP computer code, which is a plane-wave pseudopotential formalism based on density functional theory, aided by the Materials Studio graphical front−end interface.

Coloration Property Test. Photochromism of the *h*-MoO_3 nanobelt suspension was assessed using a sealed single-compartment cell (1.0 cm thickness) with two quartz windows. The suspension was diluted to a concentration of 1.0×10^{-3} mmol mL^{-1}. Afterward, the suspension was bubbled with N_2 gas, and the cell was tightly sealed. A 450 W high-pressure lamp was used as the excitation source.

The *h*-MoO_3 nanobelts coated film for electrochromic measurement was prepared by dropping the suspension (0.3 mL) with a MoO_3 concentration of 4 mg mL^{-1} onto the surface of a cleaned ITO glass and then drying at room temperature for 48 h. Electrochromic properties of the MoO_3 nanobelt coated film were studied by a three electrode electrochemical cell with 1.0 M lithium perchlorate ($LiClO_4$) in propylene carbonate (PC) as the electrolyte. In all measurements, cyclic voltammetry (CV) and constant voltage characteristics were recorded with an electrochemical station (CHI 660B). The MoO_3 nanobelt film was vertically inserted into the electrolyte and acted as the working electrode, the graphite plate acted as the counter electrode, and the saturated calomel electrode (SCE) acted as the reference electrode. CV curves were measured between +1.0 and −1.0 V with a sweep rate of 0.1 V s^{-1} and recorded every 100 cycles to the 1200th cycle.

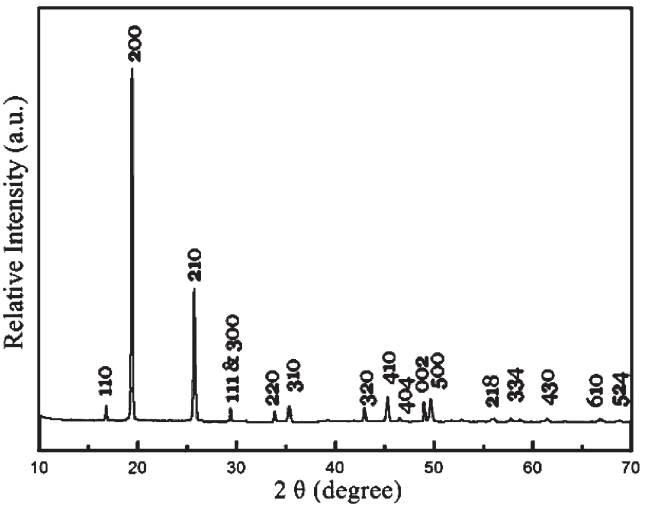

Figure 1. XRD pattern of as-prepared hexagonal *h*-MoO_3 nanobelts.

3. Results and Discussion

3.1. Structural Characterization and Growth Mechanism of *h*-MoO_3 Nanobelts. The *h*-MoO_3 sample was obtained via a hydrothermal decomposition reaction of peroxomolybdate precursor. The phase and crystallographic structure of the MoO_3 products were well-characterized using powder XRD technique. Figure 1 demonstrates the XRD pattern of as-synthesized nanobelts, which is in good agreement with the hexagonal *h*-MoO_3 phase with lattice parameters of a = 10.53 Å and c = 14.97 Å (JCPDS card No. 21-0569, space group *P*63). No other phases are detected in final products. In the XRD pattern, the strong diffraction peak of (200) relative to other planes indicates that most nanobelts lie on the holder with {100} planes, and they have the preferential growth in the [001] direction.

Through the hydrothermal decomposition of precursor crystals with the presence of sodium nitrate, we obtained well-defined *h*-MoO_3 nanobelts. The typical SEM image (Figure 2A) gives a panoramic picture of the product, revealing that the product consists almost entirely of nanobelts. The inset of Figure 2A provides a selected, magnified single nanobelt from the cross-section view, where the natural curving morphology indicates the belt-like structure and the thickness of a typical nanobelt is 20−30 nm. The TEM image of the nanobelts shows that they have an average diameter of 150 nm and a length up to micrometers, as seen in Figure 2B. Figure 2C reveals the TEM image of an individual nanobelt, and its corresponding HRTEM and SAED patterns before and after

(23) Segawa, K.; Ooga, K.; Kurusu, Y. *Bull. Chem. Soc. Jpn.* **1984**, *57*, 2721.

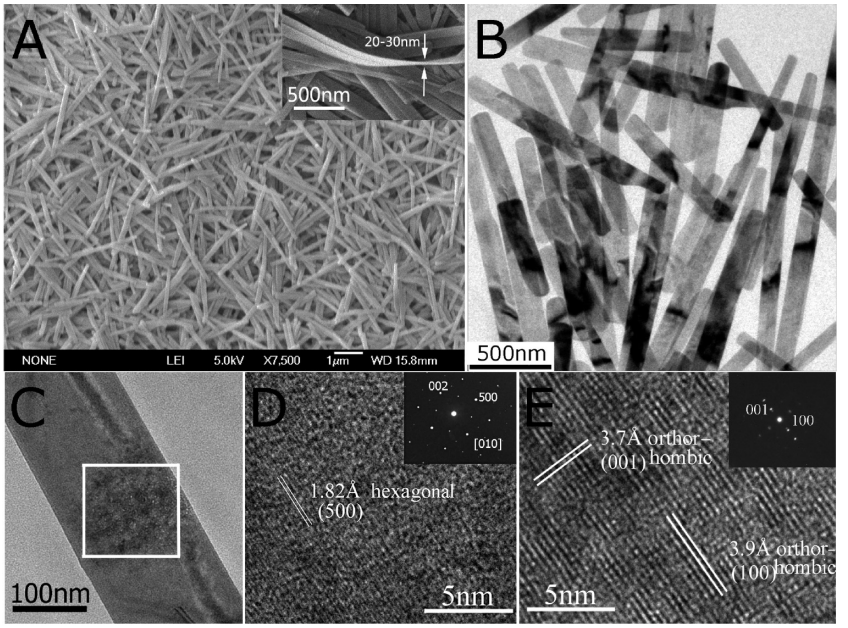

Figure 2. (A) SEM image (inset is a cross-section view of single nanobelt) and (B) TEM image of as-prepared *h*-MoO_3 nanobelts; (C) an individual *h*-MoO_3 nanobelt; and its HRTEM image showing a change from a crystalline (D) to recrystallization (E) state under electron irradiation (inset is the corresponding selected area electron diffraction pattern).

electron irradiation are shown in Figure 2D,E respectively. Partly because of its instability, the correlative reports on the periodical lattice planes and electron diffraction of metastable *h*-MoO_3 nanoparticles are few,[24] and our results therefore would exhibit more information about its crystalline structure. The neighboring lattice spacing along the radial direction is determined to be 1.82 Å and is close to the distance of 1.8240 Å between (500) planes given from standard JCPDS card. The spot of (100) was extincted in the electron diffraction pattern (the inset of Figure 2D), and all the observed spots can be attributed to the [010] zone axis diffraction, as well as the growth of nanowires along the [001] direction. The results verify the single-crystalline nature of the nanobelts. A striking feature of the nanobelts is that they are prone to becoming recrystallized under the electron irradiation, as observed in Figure 2E. Within 4−5 min upon irradiation, all periodical lattices are changed, and the new crystalline nature of the nanobelt is also revealed by the lattice fringes of 3.7 Å and 3.9 Å, assigned to the (001) and (100) crystal planes of orthorhombic α-MoO_3. The corresponding SAED pattern presents several faint spots with vague halo rings, where the spots indexed into the (100) and (001) planes are also typical electron diffraction spots as reported results in previous literature. It is reasonable that the thin nanobelts lose the crystalline state under the HRTEM rather than TEM observation because of the stronger electron beam energy in the former, and a similar phenomenon has been observed on metastable hexagonal phase $V_{0.13}Mo_{0.87}O_{2.935}$ nanowires[25] which has the same crystalline structure as *h*-MoO_3. The area in the white pane of Figure 2C gives the TEM image after the electron bombardment, where the crystallinity is obviously different from the rest of the nanobelt. Early works have shown that hexagonal *h*-MoO_3 could be stable even up to 440 °C, and in our case (see Figure S1 in the Supporting Information), the *h*-MoO_3 nanobelts start to transform irreversibly into the α-MoO_3 phase at 400 °C which was confirmed by the differential scanning calorimetry (DSC), giving one hint that as-synthesized *h*-MoO_3 is stable enough for further application at room temperature and could withstand a jump over a wide temperature range.

In regard to the reaction approach, peroxomolybdate solution was preprepared by pure Mo powder dissolved in H_2O_2 aqueous solution as described with a species of $MoO_2(OH)(OOH)$.[23] The chemical reaction can be formulated as shown in eq 1

$$Mo + 4H_2O_2 \rightarrow MoO_2(OH)(OOH) + 3H_2O \qquad (1)$$

and the followed thermolysis reaction via loss of one molecule of water and half a molecule of oxygen gas to form crystalline MoO_3 as shown in eq 2

$$2MoO_2(OH)(OOH) \rightarrow 2MoO_3 + 2H_2O + O_2 \qquad (2)$$

Obviously, according to the crystalline structure of MoO_3 polymorphs, the deoxidation, condensation and further dehydration of the peroxy structure are responsible for the formation of the [MoO_6] octahedra with either vertex sharing or edge sharing arrangements, which is similar to the dehydration and the following condensation that acted on the forming ferrihydrite phase.[26]

(24) Dhage, S. R.; Hassan, M. S.; Yang, O. B. *Mater. Chem. Phys.* **2009**, *114*, 511.
(25) Hu, X. K.; Ma, D. K.; Liang, J.; Xie, Q.; Zhu, Y; Qian, Y. T. *J. Phys. Chem. C* **2007**, *111*, 5882.
(26) Wu, Z. C.; Zhang, M.; Yu, K.; Zhang, S. D.; Xie, Y. *Chem.—Eur. J.* **2008**, *14*, 5346.

Scheme 2. Schematic Illustration Showing the Formation of the MoO_3 Polymorphs

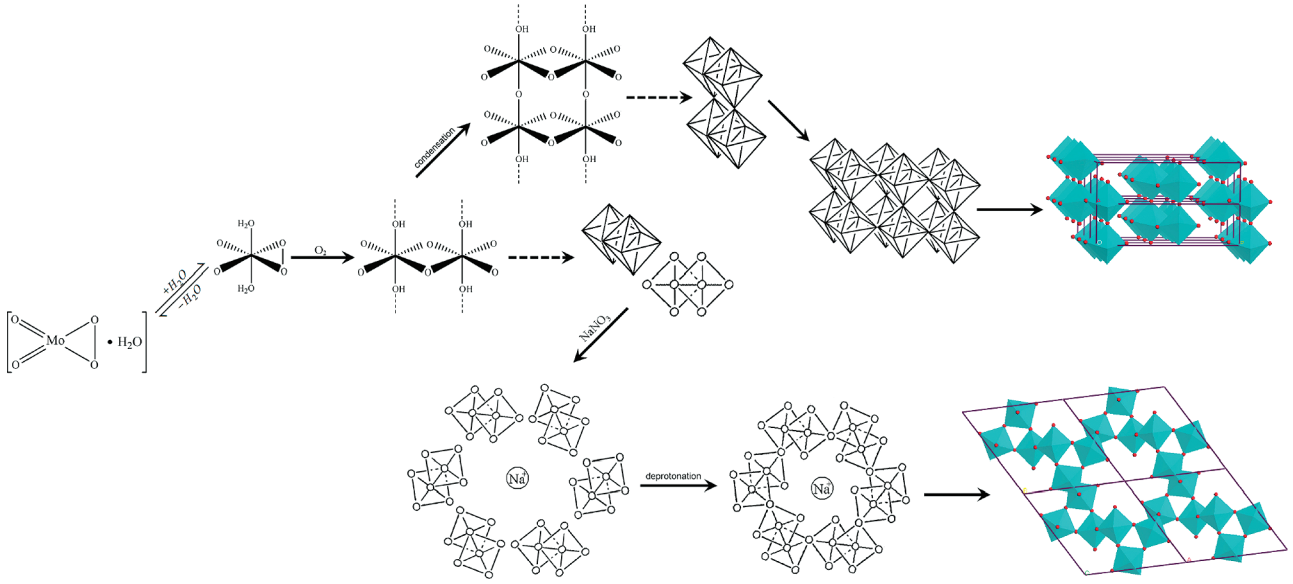

Further condensation results in zigzag chains as the buliding block along the *c* axis arranged into both α-MoO_3 and *h*-MoO_3 structures. Our method is based on treating the peroxomolybdate precurser in the presence of $NaNO_3$ as mineralizer under hydrothermal conditions. And a control experiment demonstrated that hydrothermal reaction of peroxomolybdate precurser without minerilizer of $NaNO_3$ only obtains irregular α-MoO_3 nanobelts,[27,28] suggesting that $NaNO_3$ plays a decisive role in the formation of *h*-MoO_3 nanobelts. As one might expect, in the pure peroxomolybdate solution, [MoO_6] octahedra readily share two vertexes at the para position, so that zigzag chains connect via an oxolation mode to produce layers in MoO_3 stoichiometry. These layers are stacked in a staggered arrangement and are only held together by weak van der Waals forces to produce a three-dimensional framework of α-MoO_3. Nevertheless, the existence of $NaNO_3$ in peroxomolybdate precursor may change the oxolation mode because of the electrostatic interaction existing between Na cation and oxygen atom. For more oxygen atoms interacting with Na cation, [MoO_6] octahedra share two vertexes at the ortho-position, and thus zigzag chains interlink each other through the *cis*-position, leading to the spontaneous arrangement of hexagonal crystalline structure with large one-dimensional tunnels (Scheme 2). When other inorganic salts such as Na_2SO_4 and Na_2HPO_4 were used to replace $NaNO_3$ in the reaction system, no solid product was obtained. Meanwhile, if the inorganic salts such as NaCl and KNO_3 were used to replace $NaNO_3$, we only obtained a mixture of *h*-MoO_3 and α-MoO_3. In this respect, it is confirmable that a key function of $NaNO_3$ as a mineralizer in ensuring the formation of metastable phase *h*-MoO_3. When Na_2SO_4 or Na_2HPO_4 substituted for $NaNO_3$, the absorption of larger SO_4^{2-} and HPO_4^{2-} ions on precursor molecules may increase the structural stresses of the crystal nucleus and hence result in instability of the nucleation. At the same time, these divalent anions also probably increase the ionic strength of the surrounding medium and the surface charge density at the precursor interface to form electrostatic screening,[29] which would interfere with the arrangement process of precuesor molecules and lead to no solid product ultimately. On the other hand, cations in the mineralizers may also play some roles in influencing the nucleation and growth of MoO_3 nanostructures. In such a hydrothermal process, K^+ or Na^+ cations, in the form of hydrated ions in aqueous solution, may be taken as the bond bridge between the growth units to form a crystal nucleus.[30] Because the hydrated ionic radii of the Na^+ ion (0.36 nm) is larger than that of the K^+ ion (0.24 nm), every Na^+ hydrated ion is able to attract more precursor clusters than the K^+ hydrated ion. Thus, at the same concentration of mineralizers, the Na^+ cations could dramatically influence the condensation and further dehydration of precursors as well as MoO_3 crystal nucleus. Moreover, the larger exchange capacity of the hydrated K^+ ions than that of hydrated Na^+ ions indicates that a coordination substitution reaction readily occurs between the water molecules in K^+ hydrated ions and the surrounding precursor molecules, which is also attributed to accelerating the bond formation of MoO_3 zigzag chains and ultimately causes the rapid nucleation of stable phase α-MoO_3. Simultaneously, the existence of $NaNO_3$ may also influence the morphology of the products (see Figure S2 in the Supporting Information) and be important to stabilize the hexagonal tunnels as previous literature reported.[31] It is well-known that XPS is a very useful method in determination of the chemical compositions

(27) Fang, L.; Shu, Y.; Wang, A.; Zhang, T. *J. Phys. Chem. C* **2007**, *111*, 2401.
(28) Hu, B.; Mai, L.; Chen, W.; Yang, F. *ACS Nano* **2009**, *3*, 478.
(29) Kulkarni, A. M.; Zukoski, C. F. *Langmuir* **2002**, *18*, 3090.
(30) Wang, B. G.; Shi, E. W.; Zhong, W. Z. *Cryst. Res. Technol.* **1998**, *33*, 937.
(31) Muraoka, Y.; Grenter, J. C.; Petit, S.; Pouchard, M. *Solid State Sci.* **1999**, *1*, 133.

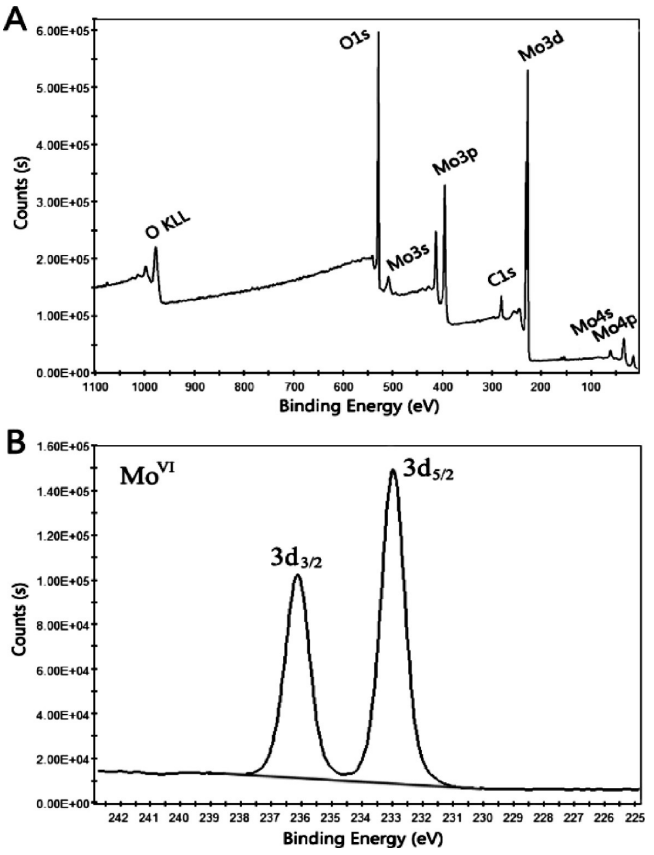

Figure 3. XPS spectrum of as-obtained *h*-MoO_3: (A) survey spectrum and (B) Mo 3d core level region.

and their chemical states of material surfaces. In our case, the XPS is applied to analysis of the residual amount of $NaNO_3$ and valence of Mo atoms. The XPS survey spectrum for the obtained *h*-MoO_3 nanobelts as shown in Figure 3A indicated that no Na cations existed. The Mo 3d spectrum (Figure 3B) presents the 5/2−3/2 spin−orbit doublet for the Mo valence state, where the intense doublet at EB(Mo $3d_{5/2}$) = 232.8 eV and EB(Mo $3d_{3/2}$) = 235.9 eV corresponds to Mo^{6+}, in close agreement with the datas found in the literature.[32] If residual Na cations occupy the tunnel sites, the charge should be compensated by Mo vacancies as Mo^{5+}, and then the color of our sample would be not yellowish white but bluish (the characteristic color of Mo^{5+}). Hence, we assume that, as a mineralizer, a few Na cations could stabilize the hexagonal tunnels at the initial stage and promote the formation of the *h*-MoO_3 phase, strapped away from the large hexagonal tunnels via repeated water washed. The different concentration of nitrate ions may form different complexes with $MoO_2(OH)(OOH)$ by condensation and dehydration, thus influence the growth rate of [MoO_6] units, and have different effects on the formation rate of various crystal faces. In other words, our experimental data leads to the proposal that the specific interaction between sodium nitrates and crystal surfaces might play an important role in controlling the morphology of the final crystals.

(32) Nefedov, V. I.; Firsov, M. N.; Shaplygin, I. S. *J. Electron Spectrosc. Relat. Phenom.* **1982**, *26*, 65.

3.2. Optical and Photochromism Properties of the MoO_3 Nanobelts. The optical absorption properties of a semiconductor, which are relevant to the electronic structure features, are recognized as key factors in determining its photoreaction activities. As Figure 4A,B show, the optical properties of as-prepared *h*-MoO_3 and α-MoO_3 (see Figure S3 in the Supporting Information) nanobelts were characterized by UV−vis absorption spectra, and the result indicates that both MoO_3 nanobelts display photoabsorption properties from the UV light region to the visible light absorption shorter than 500 nm. The steep shape of the spectra indicated that the visible light absorption was due to the bandgap transition, with 450 nm of α-MoO_3 and 470 nm of *h*-MoO_3, corresponding to a bandgap of 2.76 and 2.64 eV, respectively, as experimental data. The calculated band structures of both the α-MoO_3 and the *h*-MoO_3 phase (see Figure S4 in the Supporting Information), where all energy values are taken with respect to the Fermi level such that negative energies refer to valence bands whereas positive values characterize conduction bands, show that the calculated bandgaps are 2.59 eV for α-MoO_3 and 2.65 eV for *h*-MoO_3. Though we are not aware of any published values of the *h*-MoO_3 bandgap, the consistency between the calculated and observed values reveals that the obtained *h*-MoO_3 bandgap value here is reasonable and credible. Considering the similar bandgap and optical absorption properties of the two MoO_3 polymorphs, are there similar features for photochemical applications?

It is worth investigating color changes in metastable phase *h*-MoO_3 material upon light excitation inasmuch as that the stable phase α-MoO_3 is well-known for its photochromic behavior;[6] the color can be reversibly switched by photoexcited hole−electron pairs from the transparent state to blue, which is the characteristic color indicating a mixture of low valent Mo atoms and Mo(VI). In this work, we observed the reversible color changes in response to on-and-off of UV irradiation utilizing the colloidal nanobelt suspension of hexagonal *h*-MoO_3 and orthorhombic α-MoO_3. UV−vis absorption spectra of the nanobelt suspension for virgin, coloration, and bleached states are contrastively displayed in Figure 4C, D. As a result, the hexagonal MoO_3 nanobelts show a stronger photochromic effect than that of α-MoO_3 nanobelts by direct observation. As seen in the evolution of wide-ranging absorption (Figure 4D), the milky suspension of hexagonal MoO_3 nanobelts turned visibly blue after UV irradiation for 20 min. By introducing the absorption spectra, the change in absorbance is apparently seen across the visible range, and the largest change occurs from 600 to 800 nm. For example, a dramatic change of absorbance at 685 nm is ~0.65 after the 20 min irradiation. When the colored sample was stored under dark conditions, the color gradually bleached and eventually vanished (after about 240 min under the present conditions), hence returning to the virgin state. The chromaticity of the *h*-MoO_3 nanobelt suspension presents a milky white color in the bleached state and a blue color in the colorated state, so that the chromatism is

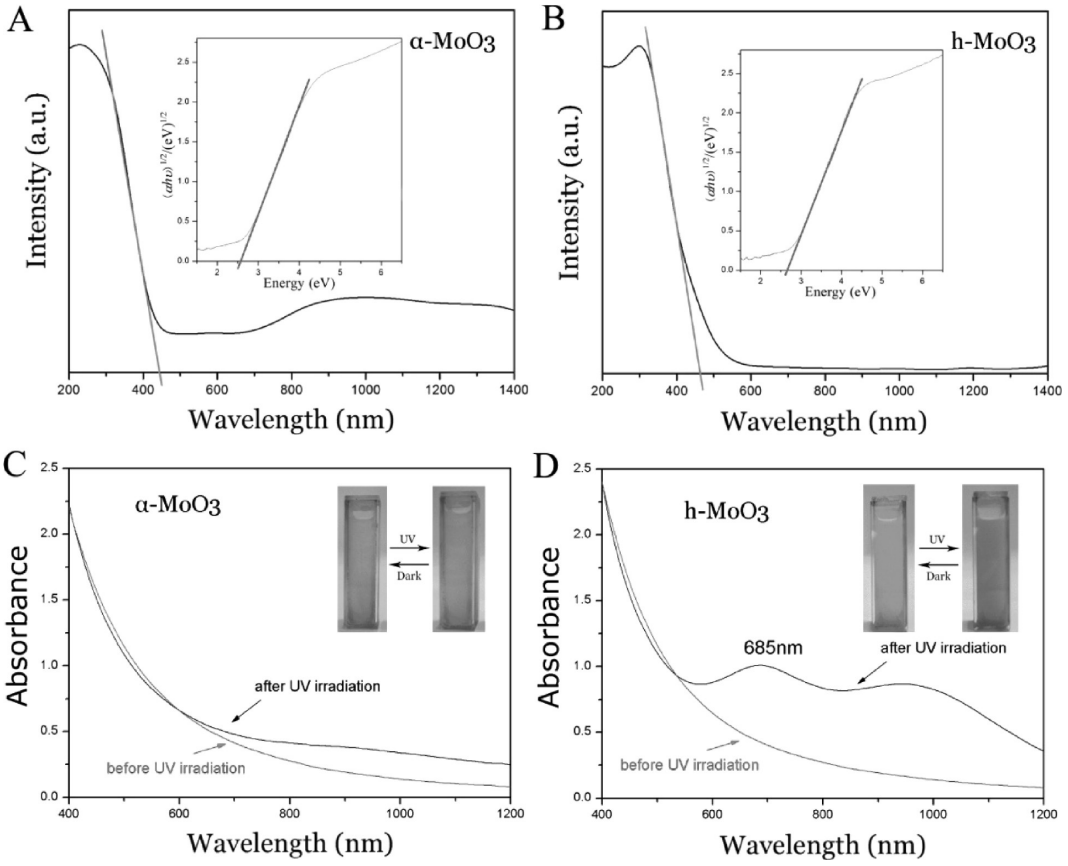

Figure 4. Typical UV−vis diffuse reflectance spectra of (A) orthorhombic α-MoO_3, (B) hexagonal MoO_3 and UV−vis spectra of the nanobelt suspension of (C) orthorhombic α-MoO_3, and (D) hexagonal MoO_3 (insets show the photochromism phenomena).

considerably obvious on observer's visual sensitivity. The coloration/bleaching could be repeated at least several times, as confirmed in this experiment. By contrast, a series of UV−vis spectra of α-MoO_3 nanobelts were also measured under the same irradiation conditions, and the results are shown in Figure 4C. The change of absorbance at 700 nm is only 0.2 for the α-MoO_3 nanobelt suspension after UV irradiation for 20 min, which exhibits a faint color change.

Up to the present, a number of studies have been carried out on the photochromism performance, and a model of double insertion/extraction of ions and electrons was developed to elucidate the photochromic mechanism of main transition metal oxides,[6] especially for MoO_3 and WO_3. The corresponding photochromic reaction process can be described by eqs 3−6. When the oxide suspensions are irradiated with UV light ($h\nu \geq E_g$), electrons and holes are generated (eq 3). Then the necessary protons for the coloration can be obtained from the reaction of the adsorbed water with holes (eq 4). Subsequently the produced protons can diffuse into the tunnels and cavities of the *h*-MoO_3 lattice, whereas the oxygen radicals may occupy the vacancy sites inside the sample or bind to each other to escape into the ambient media in molecular form. The photogenerated electrons are excited into the conduction band and then react with MoO_3 and the counterions (i.e., protons) to form hydrogen molybdenum bronze ($H_xMo^{V}_xMo^{VI}_{1-x}O_3$) (eq 5). As a result, the suspension turns blue due to the intervalence-charge transfer from the newly formed Mo^{5+} (valence band) to adjacent Mo^{6+} (conduction band) (eq 6).

$$MoO_3 \xrightarrow{h\nu} MoO_3{}^{*} + e^{-} + h^{+} \tag{3}$$

$$2h^{+} + H_2O \rightarrow 2H^{+} + O \tag{4}$$

$$MoO_3 + xH^{+} + xe^{-} \rightarrow H_xMo^{VI}_{1-x}Mo^{V}_xO_3 \tag{5}$$

$$Mo^{VI}_A + Mo^{V}_B \xrightarrow{h\nu} Mo^{V}_A + Mo^{VI}_B \tag{6}$$

It is of great interest that the two types of MoO_3 nanobelts show rather different photochromic performances. In our experiment, the morphology and the mean particle sizes of the two compounds are similar, associated with the similar optical absorption properties and band structures, which mean that the differences of photoreaction activity essentially depend on intrinsic reasons correlated to detailed crystalline structure properties.

Bearing in mind that the photochromism reveals a sensitivity of the materials in response to UV irradiation, we propose that the first step for photogenerating electrons and holes (as shown in eq 3) plays a critical role in all the above steps. And this opinion could be induced by a

series of research results,[4,33,34] in which photochromic materals modified with noble metal nanoparticles would exhibit an enhanced photochromism performance, as a result of an effective electron−hole pair separation prior to the coloration reaction. Similar surface modifications of semiconductors with noble metals have been also probed into enhancing photocatalytic activities in several cases,[35,36] which give a clue that the significance of photogenerated charge carriers in photochromism is analogous to those in the photocatalysis. Thus, it is reasonable to use the photocatalytic mechanisms for explaining how cystal structures influence photochromic properties. Here, a concept is commonly accepted that structure-induced dipole moments in distorted metal−oxygen polyhedra of the tunnel structure compounds and/or static electric fields between the layers of the layered compounds are both favorable for the separation of hole−electron pairs.[10] But recent findings in the field of photocatalysis highlighted that photocatalysts with more open tunnel structures present more catalytically active. For example, such tunnel structures with distorted metal−oxygen octahedra as $BaTi_4O_9$ and $A_2Ti_6O_{13}$ (A = Na, K) exhibit more catalytical activities than a series of layered structured oxides of $K_2Ti_2O_5$, $Na_2Ti_3O_7$, $Na_2Ti_4O_9$, and $K_4Nb_6O_{17}$.[10,37] The tunnel structure and layered structure materials both possess a spatially open construction, in which the tunnel structure compounds are generally more capacious in crystal local structure. The tunnel structure could provide wider spatial locations for atom vibrations, leading to higher momentary polarizing fields that can work as accelerators for electron−hole separation.[10] Accordingly, except for the well-known effect of band for the same compound with varied structures, the crystalline structure openness degrees of MoO_3 are believed to be closely associated with its photochromic activity.

The concept of crystal packing factor (PF)[10,38] won acceptance as a universal model for structure-dependent photocatalytic activity and introduced analyzing the photocatalytic difference of materials with similar band structure, crystalline structure, or chemical composition. This model indicates that a lower packing factor, corresponding to a higher structure openness degree, leads to a higher ability of photoinduced electron−hole separation and commonly better photochemical activity.[30] In our case, packing factors of the *h*-MoO_3 and α-MoO_3 could be computed via dividing the sum of spherical volumes by the unit cell volume, as seen in the following equation:

$$\mathrm{PF} = Z(xV_A + yV_B + zV_C)/V_{cell}$$

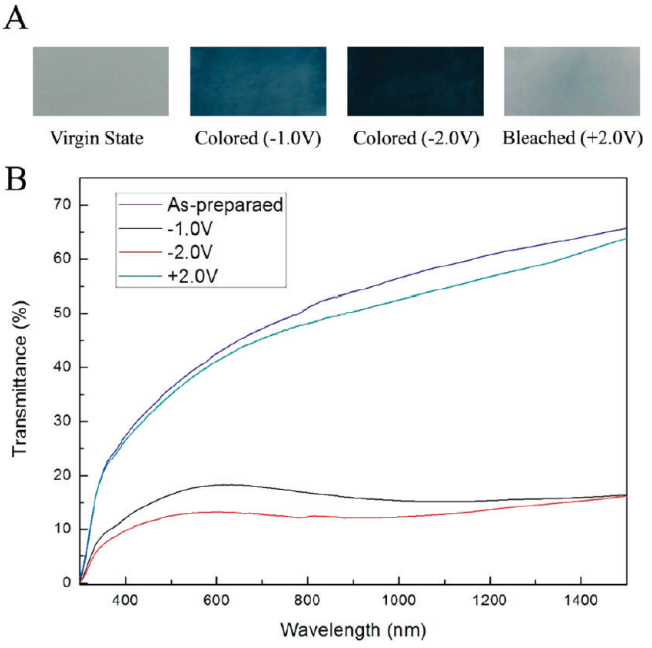

Figure 5. (A) Color changes of the hexagonal MoO_3 nanobelt film at different voltages with 1.0 M lithium perchlorate ($LiClO_4$) in propylene carbonate (PC) as the electrolyte: the as-prepared film, colored at −1.0 V, colored at −2.0 V and bleached at 2.0 V. (B) Corresponding UV−vis transmittance spectra for electrochromic phenomena of the hexagonal MoO_3 nanobelt film.

where Z is the number of the formula unit in one unit cell of a semiconductor ($A_xB_yC_z$); V_A, V_B, and V_C are ion volumes calculated by assuming spherical ions with a Shannon's radius that depends on the coordination number; and V_{cell} is the cell volume. In this work, two types of MoO_3 are assumed with the same ion volumes of molybdenum and oxygen, and the Z values are 4 and 6, while the V_{cell} values are 200 Å^3 and 357 Å^3 for α-MoO_3 and *h*-MoO_3, respectively. The calculated packing factor value of *h*-MoO_3:α-MoO_3 is 1:1.19, revealing that the structure openness degree of *h*-MoO_3 is higher than that of α-MoO_3, which means a higher mobility for photoinduced electron−hole separation in photochromic reaction.

In addition, the photochemistry activity often depends on the distortion of the metal−oxygen polyhedron in crystalline structures.[39,40] The bridge oxygen angle of Mo−O−Mo is 157.6° in *h*-MoO_3, slightly smaller than that in α-MoO_3 (167.7°), as a relatively larger distortion in the unit cell of *h*-MoO_3, which may attribute to electron−hole generated inside the crystal easily and transferring to the surface, hence resulting in an enhanced photochromic property.

Another direct evidence for generatation of electron−holes can be provided by their photocatalytic properties. We investigated the photocatalytic activity of the two types of MoO_3 nanobelts for the degradation of Rhodamine B (RhB); the same trend as photochromism performed by *h*-MoO_3 nanobelts was observed (see Figure S5 in the Supporting Information).

(33) He, T.; Ma, Y.; Cao, Y.; Jiang, P.; Zhang, X.; Yang, W.; Yao, J. N. *Langmuir* **2001**, *17*, 8024.
(34) Yao, J. N.; Yang, Y. A.; Loo, B. H. *J. Phys. Chem. B* **1998**, *102*, 1856.
(35) Fox, M. A.; Dulay, M. T. *Chem. Rev.* **1993**, *93*, 341.
(36) Linsebigler, A. L.; Lu, G.; Yates, J. T., Jr. *Chem. Rev.* **1995**, *95*, 735.
(37) Templeton, D.; Dauben, C. *J. Chem. Phys.* **1960**, *32*, 1515.
(38) Lin, X.; Huang, F. Q.; Wang, W.; Shan, Z.; Shi, J. *Dyes Pigm.* **2008**, *78*, 39.
(39) Zhang, L.; Chen, D.; Jiao, X. *J. Phys. Chem. B* **2006**, *110*, 2668.
(40) Kurihara, K.; Okutomi, H.; Miseki, Y.; Kato, H.; Kudo, A. *Chem. Lett.* **2006**, *35*, 274.

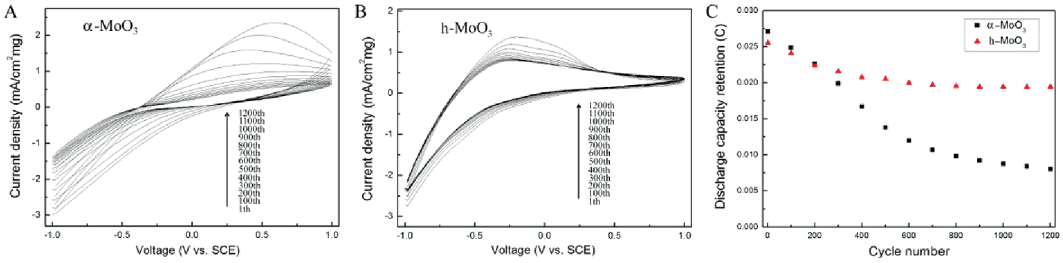

Figure 6. CV curves of the (A) orthorhombic α-MoO_3 and (B) *h*-MoO_3 nanobelts coated film for 1200th cycles and measured in 1.0 M $LiClO_4$/PC solution with a sweep rate of 0.1 V/s and (C) discharge capacity retention comparison between the two type MoO_3 nanobelts coated film after different CV cycles.

3.3. Electrochromic Properties of the *h*-MoO_3 Nanobelt Film. The electrochromic properties were performed by using organic electrolyte containing $LiClO_4$ and occurred via Li^+ ion insertion into the host electrode structure. Figure 5A displays the observed electrochromic phenomena of the as-prepared *h*-MoO_3 nanobelt film. It can be seen that the as-prepared MoO_3 nanobelt film is almost colorless and transparent enough. When applying a voltage of −1.0 V, the film displayed a blue color immediately. And a saturated color in deep blue was exhibited all over the film when the applied voltage increased to −2.0 V. The generation of a color change that requires little or no additional input of power is the unique energy saving memory effect of electrochromic films, which is absent in other devices such as liquid crystal displays (LCDs) that persist with a constant input of power to display their colors,[41] indicateing that *h*-MoO_3 chromogenic material is readily applicable to correlated smart window glass. The colored *h*-MoO_3 nanobelt film can retain its colors for several days after removing the applied voltages. That is, once it is charged within a very short time, the *h*-MoO_3 nanobelt film will provide long-time color displays, so significant energy savings can be realized. The bleaching ability is also of interest for active modulated smart displays or windows. When we applied a voltage of 2.0 V to the deep blue film, its color was bleached quickly and a transparent film was obtained again, which demonstrated a well cyclic performance and sensitivity in response to the electrical impulsing.

The transmittance spectra of the hexagonal MoO_3 nanobelts coated film recorded at different applied voltages was shown in Figure 5B. There are two strong and wide transmittance peaks at ~620 and 590 nm in the transmittance curves measured at −1.0 and −2.0 V, respectively, which implies that the MoO_3 nanobelt film can display from green-blue to dark blue color at different voltages. Obviously, the maximum transmittance wavelengths have a blue-shift, and the transmittance intensities decrease with the increase of the applied negative voltages within the spectra of visible light. This result is consistent with the direct observations from the electrochromic phenomena. The transmittance of the virgin *h*-MoO_3 nanobelt film is 63.0% at a wavelength of 1500 nm. At coloration potentials of −1.0 and −2.0 V, the transmittance is reduced to about 13.0%, respectively. In the bleached state, the transmittance of the film could be recovered to 59.5%. The significant modulation of the transmittance of this film in the wavelength region above 800 nm is very important, as thermal energy radiated in the IR region falls into this range. The distinct optical modulation of over 30% above 800 nm obtained here implies that the hexagonal MoO_3 is an ideal infrared switch material for the potential application in smart windows.

Several investigations expounded that the electrochromic mechanism of MoO_3 in Li^+ electrolyte can be expressed as:

$$MoO_3 + xe^- + xLi^+ \underset{\text{deintercalation}}{\overset{\text{intercalation}}{\rightleftharpoons}} Li_xMoO_3$$

The intercalation/deintercalation of electrons and charge balancing Li cations lead to the coloration/bleaching switching. The hexagonal phase of MoO_3 readily intercalates Li cations to form Li_xMoO_3 where x can be as large as 1.5,[42] and the Li^+ intercalation capacities of the MoO_3 nanobelt film directly influence the electrochromic performance.

The cyclic performances of molybdenum trioxide nanobelt coated thin films could be also characterized by cyclic voltammetry (CV) in 1.0 M $LiClO_4$/propylene carbonate (PC) electrolytes. The reduction process, accompanied by the coloration phenomena of MoO_3, involves the injection of Li cations and electrons into MoO_3 nanobelts. In comparison, we measured the cyclic voltammetry curves of both hexagonal and orthorhombic MoO_3 nanobelt films, recorded every 100 cycles at room temperature, and the results are shown in Figure 6A,B. The current densities performed by the α-MoO_3 nanobelt film are sharply decreased in the continuous charge and discharge curves, while for *h*-MoO_3 nanobelt film, only a slight reduction in the current densities within the first 300 cycles is observed and the current densities are almost constant in the rest cycles. The deintercalation charges extracted for different cycles are depicted in Figure 6C, indicating that the charge capacity of the *h*-MoO_3 nanobelt film decreases slightly less than that of α-MoO_3 nanobelt film and becomes almost constant after 300 cycles, which is consistent with the CV results. Both the

(41) Wang, J. M.; Khoo, E.; Lee, P. S.; Ma, J. *J. Phys. Chem. C* **2008**, *112*, 14306.

(42) Guo, J. D.; Zavalij, P.; Whittingham, M. S. *J. Solid State Chem.* **1995**, *117*, 323.

Scheme 3. Schematic Representation of Li Cation Possible Intercalation Sites in *h*-MoO_3

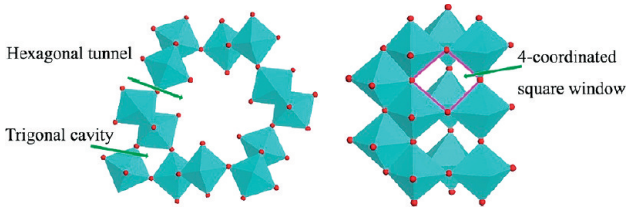

CV curves and charge retention curves indicate the high stability of the as-prepared crystalline hexagonal MoO_3 nanobelt electrochromic film.

The enhanced electrochromic properties of the hexagonal MoO_3 nanobelt film should be also attributed to its tunnel structure where structure openness degree is higher than that in the layered structure of orthorhombic α-MoO_3, resulting in Li cations could easily inserting/extracting and moving in large tunnels. Due to the many vacancies in the tunnel structure, the *h*-MoO_3 also exhibited a high capacity on Li^+ ion battery application.[43] Recently, research[9] in the field of electrochromism was reported on the possible sites for the Li^+ ion occupation in hexagonal WO_3, and the structure similarities between *h*-WO_3 and *h*-MoO_3 give some hints toward the explanation of the electrochromic performance. As a small cation, Li could occupy three possible locations in these hexagonal structures, which are the trigonal cavity, hexagonal window, and the four-coordinated square window, shown in Scheme 3. According to the reported results, the electrochromism is mainly due to the occupancy of Li^+ ions in hexagonal windows as well as in four-coordinated square windows, and Li^+ ions enter into all the cavities through the hexagonal tunnels. Thus, we deduce that the larger hexagonal tunnels in *h*-MoO_3 worked as the widening intercalation path for Li^+ ion insertion/extraction and diffusion are favorable for the reversibility of the switching process.

(43) Song, J.; Wang, X.; Ni, X.; Zheng, H. G.; Zhang, Z. D.; Ji, M.; Shen, T.; Wang, X. W. *Mater. Res. Bull.* **2005**, *40*, 1751.

To sum up, a more open structure compound of various polymorphs could provide an accelerated photoinduced electron−hole separation for photochromic and facile diffusion pathways for cation intercalation in electrochromism, which is an important factor to remind us one clue on searching for new chromogenic materials in these types of transition metal oxides.

4. Conclusion

Novel metastable hexagonal phase MoO_3 nanobelts with large-tunnel structure were prepared via a simple hydrothermal decomposition route from peroxomolybdate solutions. Sodium nitrate was found to be a mineralizer on determining the generation of the metastable phase during the deoxidation, condensation, and further dehydration process of the peroxomolybdate precusors. Enhanced photochromic and electrochromic properties of the as-obtained hexagonal *h*-MoO_3 nanobelts have been investigated in comparison with the conventional stable phase of orthorhombic α-MoO_3 nanobelts. The intrinsical structure difference between the tunnel structure of *h*-MoO_3 and the layered structure of α-MoO_3 is proposed to influence their photochromic and electrochromic properties. In fact, the exciting performances of the prepared hexagonal *h*-MoO_3 are expected to become available in the foreseeable future for wide applications in the areas of color displays and smart window devices.

Acknowledgment. This work was financially supported by the National Basic Research Program of China (No. 2009CB939901).

Supporting Information Available: Morphology differences and DTA curve of *h*-MoO_3 samples; experiments, SEM and TEM images, and SAED pattern of orthorhombic α-MoO_3 nanobelts; calculated band structures of *h*-MoO_3 and α-MoO_3 nanobelts; comparative study on *h*-MoO_3 and α-MoO_3 nanobelts for photodegradation of of Rhodamine B (RhB), and electrochromic performance of *h*-MoO_3 microprism sample (PDF). This material is available free of charge via the Internet at http://pubs.acs.org.